European Journal of Mechanics / A Solids 109 (2025) 105433

Contents lists available at ScienceDirect

European Journal of Mechanics / A Solids

journal homepage: www.elsevier.com/locate/ejmsol

Full Length Article

Development of multi aluminium foam-filled crash box systems to improve crashworthiness performance of road Service vehicle

A. De Biasio [a], H. Ghasemnejad [a,*], S. Srimanosaowapak [b], J.W. Watson [c]

[a] School of Aerospace, Transport and Manufacturing (SATM), Cranfield University, MK430AL, UK
[b] National Metal and Materials Technology Center (MTEC), Pathum Thani 12120, Thailand
[c] Cranfield Impact Centre (CIC), Cranfield, MK43 0AL, UK

ARTICLE INFO

Keywords:
Crashworthiness
Honeycomb
Aluminium foam
Stiffener reinforcements
Impact

ABSTRACT

Honeycomb crash absorbers are known as mechanical energy-absorbing systems in both automotive and aerospace industries. However, the gap of knowledge in the transverse impacts of multi-foam-filled or stiffener-reinforced honeycombs is still unfilled. This paper investigates the energy absorption process in large crash boxes applied onto a road maintenance vehicle, exploring four aluminium honeycomb absorbers with design factors like added aluminium foam, corrugated sheet thicknesses, and stiffener reinforcements. The optimised foam-filled honeycomb structures are analysed for four crash scenarios in two different directions; frontal impact (T-direction) and lateral impact (L-direction) subjected to 50 km/h crash speed. The objective of this research is to identify the most efficient design that achieves a maximum acceleration of up to 20g while absorbing a specific energy of 145 kJ. The FE models were developed in ABAQUS to explore various scenarios related to damage zones, impact energy capabilities, and multi-foam-filled crash boxes. Finally, the lightest design of honeycomb absorbers which can maximise energy absorption while maintaining acceleration below the specified threshold of 20g will be recommended.

1. Introduction

Safety measures are vital, particularly in high-risk regions like Thailand with unsafe roads and limited safety equipment in the areas under construction and maintenance. Honeycomb designs, prevalent in aerospace and automotive industries, involve key concepts: honeycomb density, bonded hexagonal cell units, ribbon or web, nodes, free walls, L and R directions (continuous sheet orientations), and T direction (parallel with cell openings). This efficient energy-absorbing design converts kinetic energy into internal work, featuring long strokes, uniform crushing, and superior compressive strength-to-weight ratio (Bitzer, 1997). Crashworthiness relies on quantifiable parameters such as Absorbed Energy (AE), Specific Energy Absorption (SEA), Mean Crushing Force (MCF), Peak Crushing Force (PCF), Crash Force Efficiency (CFE), Mean Acceleration (MA), Peak Acceleration (PA), Kinetic Energy (KE), Maximum Displacement (MD) and Force-Displacement (FD). Wierzbicki (1983) investigated the axial compressive strength of hexagonal cell honeycombs, and Wu et al. (Wu and Jiang, 1997) conducted experimental studies on six honeycomb types in axial quasi-static and impact loads. Levent et al. (Aktay et al., 2008) proposed numerical techniques for the transverse crush behaviour of aluminium and Nomex honeycombs. Zarei-Mahmoudabadi et al. (Zarei Mahmoudabadi and Sadighi, 2011) presented a theoretical model for the MCF of foam-filled hexagonal metal honeycombs under quasi-static loading. He et al. (He and Ma, 2015) developed a full-scale FE model of a hexagonal honeycomb energy absorber using LS-DYNA, validated with theoretical solutions and experiments. PCF decreases with change of trigger mechanisms for a controlled and stable collapse with reduced injury (Langseth et al., 1994; Rai et al., 2019). Crash tubes undergo significant plastic deformation to prevent abrupt deceleration and maintain KE transformation and deceleration below a critical threshold (Lu and Yu, 2003). An ideal collapse pattern for an aluminium structure resembles a diamond shape (Yuen and Nurick, 2008). The FD diagram exhibits elastic deformation before PCF, followed by plastic deformation with oscillations, associated with lobes, from material folding to the final region which is the densification zone (Langseth and Hopperstad, 1996). Circular-triangular nested tubes filled with aluminium foam were studied for impact using dynamic tests and numerical simulations (Wang et al., 2021). Open-cell metal foams which are preferred for crashworthiness exhibit a well-defined plateau stress σ_{pl} with plastic strength

* Corresponding author.
E-mail address: Hessam.Ghasemnejad@cranfield.ac.uk (H. Ghasemnejad).

https://doi.org/10.1016/j.euromechsol.2024.105433
Received 17 May 2024; Received in revised form 31 August 2024; Accepted 2 September 2024
Available online 3 September 2024
0997-7538/© 2024 The Authors. Published by Elsevier Masson SAS. This is an open access article under the CC BY license (http://creativecommons.org/licenses/by/4.0/).

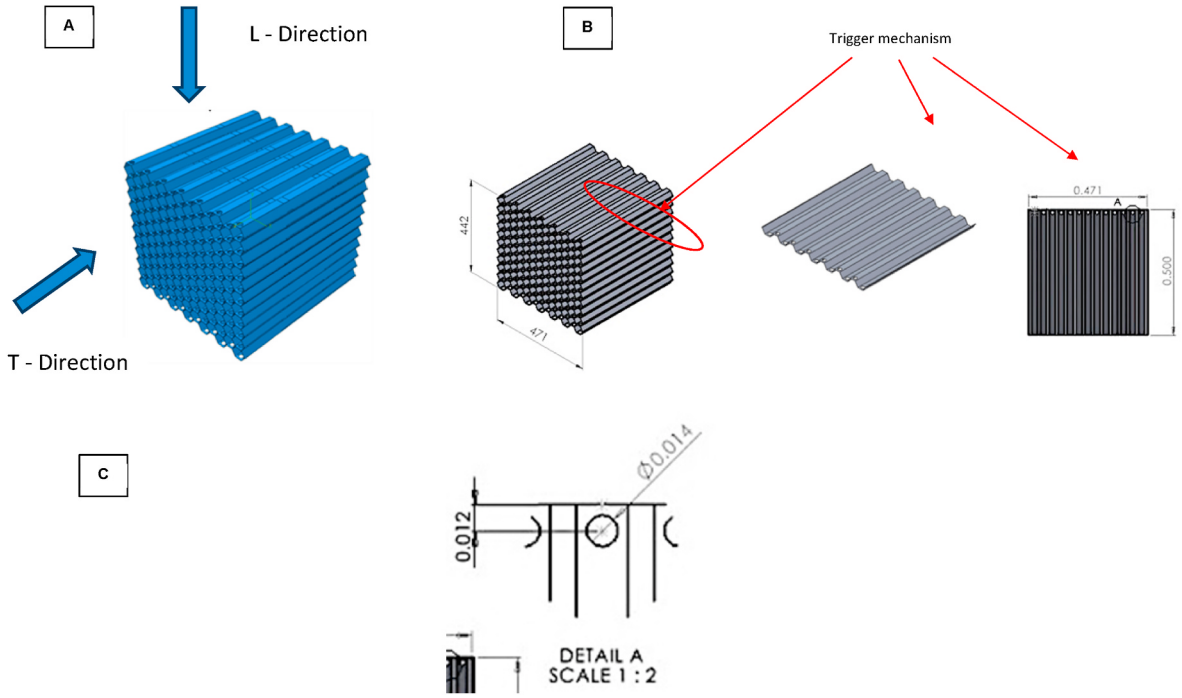


Fig. 1. A) Impact directions (T-direction is normal to the front face and L-direction is normal to the side of honeycomb absorber), B) CAD model and dimensions of the honeycomb, corrugated sheet, and C) trigger mechanism for the unreinforced honeycomb design.

Table 1
Johnson-Cook plasticity and failure model parameters.

Parameters	A [MPa]	B [MPa]	n	T_m (°C)	T_r (°C)	m	C	$\dot{\varepsilon}_{ref}$
Values	116.64	31.84	0.323	775	23.2	0.859	0.001	1
Parameters		D_1		D_2		D_3		D_4
Values		0.0749		0.3251		5.3412		0.147

Table 2
Aluminium model material parameters.

Parameters	E [GPa]	σy [MPa]	ρ [kg/m^3]	C	α_1	α_2	m	n
Values	72.4	179	350	0.3	1.5	0.36	1.17	2.13

Table 3
Dimensions of the foam-filled honeycomb and corrugated sheets, also for validation purposes.

Foam part	*Value*
Height	20 mm
Width	46.6 mm

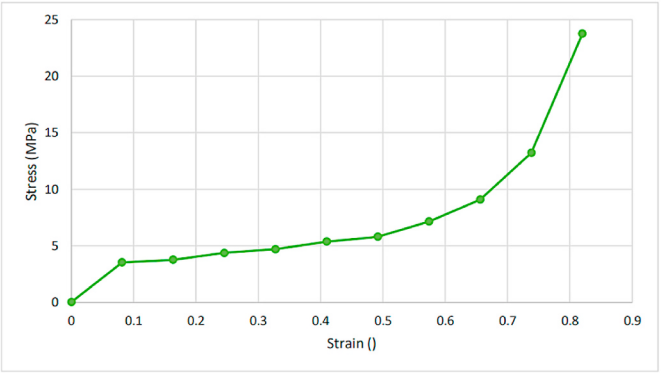


Fig. 2. Aluminium model stress-strain curve.

depending on material density (Ramamurty and Paul, 2004). Axial compression tests show that foam-filled tubes outperform empty ones in reaction loads, AE, SEA, MCF, and CFE. Extensional deformation dominates in empty honeycomb structures, and extensional deformation occurs at the welded sides. Frontal compression causes inner wall failure due to transverse forces from aluminium foams (Valente et al., 2023). Compressed structures with thin walls and aluminium foam demonstrate superior energy absorption, attributed to induced interaction effects and friction, limiting transverse displacement by developing folds in the aluminium foam (Zhang et al., 2010; Hanssen et al., 2000; Güden and Kavi, 2006; Garai et al., 2020; Pandarkar et al., 2016; Rajak et al., 2014; Li et al., 2012). Srinath et al. performed uniaxial compression tests on a steel and aluminium closed-cell foam tube and confirmed a progressive increase in MCF due to the interaction effect with the steel shell (Srinath et al., 2010).

Langseth et al. (1998) indicated that higher foam density enhances CFE, with multiple tube packing surpassing cumulative reaction loads of equivalent individual empty and foam-filled tubes. SEA increases with foam density and cell wall thickness, especially with adhesive between the foam and extrusion wall (Hanssen et al., 2000; Güden and Kavi, 2006; Garai et al., 2020; Langseth et al., 1998). Garai et al. identified adhesive bonding as the most effective joining technique (Garai et al., 2020). However, foam-filled tubes demonstrate superior CFE and SEA

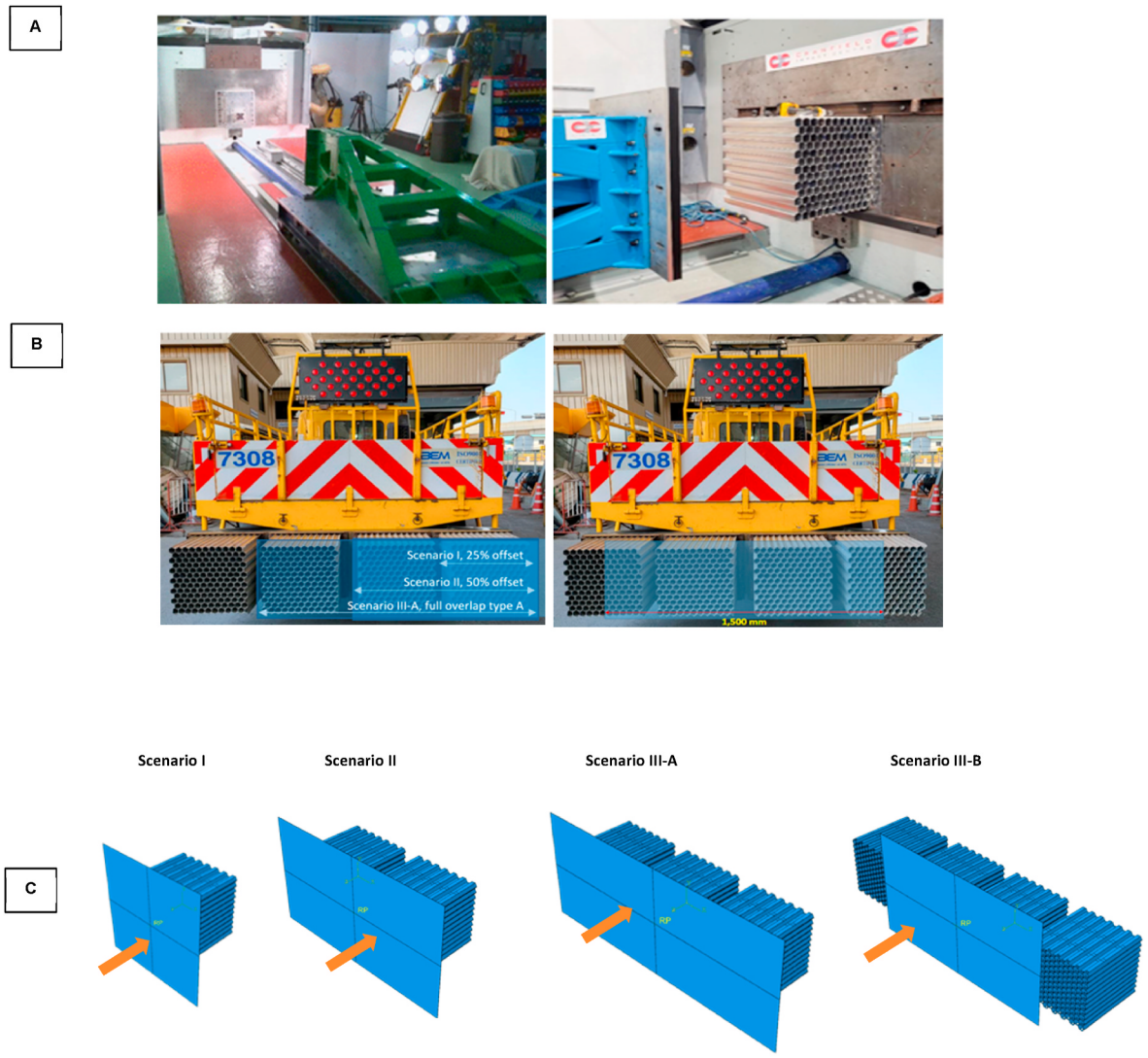


Fig. 3. A) Dynamic test set-up on an empty specimen at Cranfield Impact Centre (CIC), B) Test matrix of honeycomb absorbers, and C) Scenarios I, II and III-A, III-B.

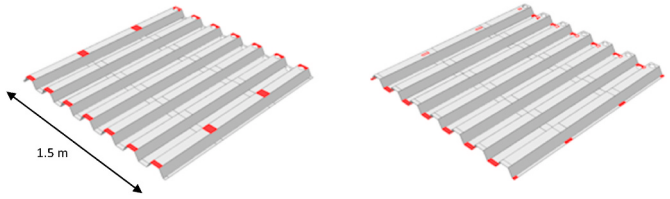


Fig. 4. Tie-constrained surfaces (in red) for modelling the welding joints. (For interpretation of the references to colour in this figure legend, the reader is referred to the Web version of this article.)

compared to empty tubes in post-crash scenarios. Linear-elastic bending occurs initially until critical stress triggers cell collapse, forming plastic hinges at the section of the maximum moment, leading to compression until walls touch, marking the densification zone (Betts et al., 2012).

This paper investigates energy absorption in large crash boxes on a road maintenance vehicle, exploring four aluminium honeycomb cases with design factors like added aluminium foam, various corrugated sheet thicknesses, and stiffener reinforcements. The ABAQUS software was used to develop the FE models exploring scenarios related to damaged zone, impact energy, and number of crash boxes. The main goal of this study is to define the lightest design of honeycomb absorbers maximising energy absorption while maintaining acceleration below the specified threshold of 20 g for safety requirements.

2. Experimental studies

This paper mainly concentrates on numerical studies and for validation purposes relies on previous authors' experimental data (Valente et al., 2023; Nicoud et al., 2023; Valente, 2021). This study explores the behaviour of quasi-static and impact scenarios of empty and foam-filled honeycomb crash boxes by assessing the influence of open-cell aluminium foam. Mechanical properties were determined through experimental tests using aluminium alloy (1100 series, H14 temper) for corrugated sheets and A356.2-Sr alloy for open-cell aluminium foam, (Valente et al., 2023; Nicoud et al., 2023; Valente, 2021). Dynamic impact tests were employed using consistent impactor shapes for T and L-direction scenarios, with acceleration measurements from the impactor determining load values. The MCF (σ_{pl}) represents the constant nominal stress where the absorber collapses plastically, up to a nominal strain ε_D beyond which the structure enters a densification zone, and stress increases steeply. PCF slightly affects MCF and absorbed energy, while crushing length plays a significant role (see Fig. 1).

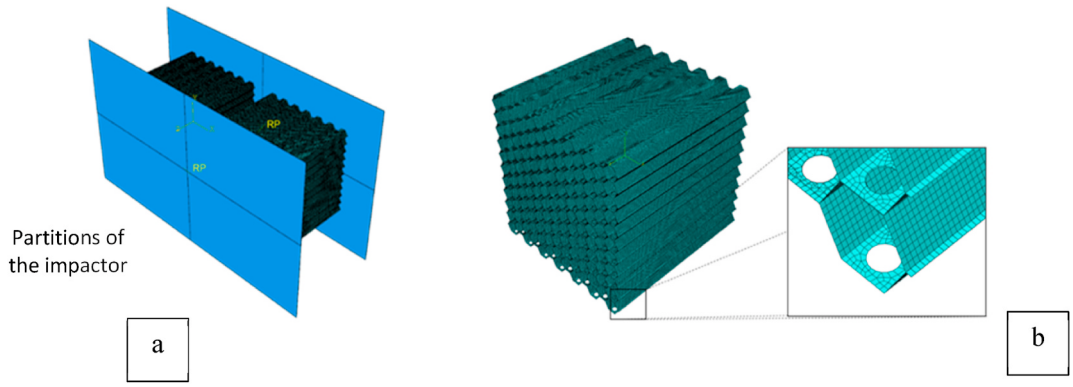


Fig. 5. a) Assembly for scenario II and b) meshed assembly systems.

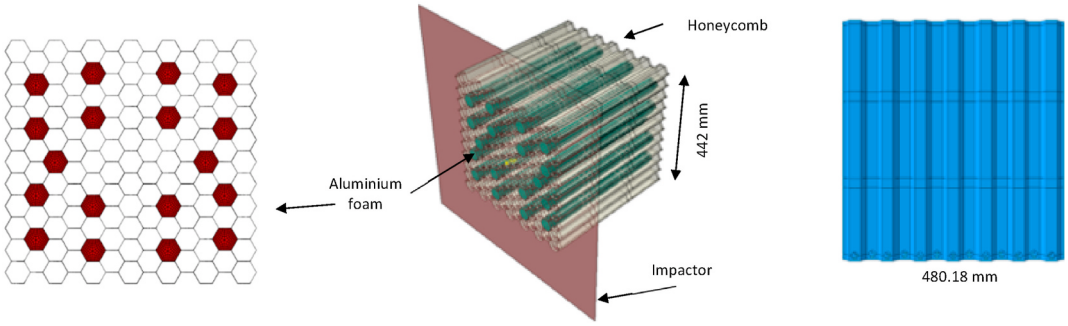


Fig. 6. Foam-filled honeycomb and corrugated sheets, also for validation purposes.

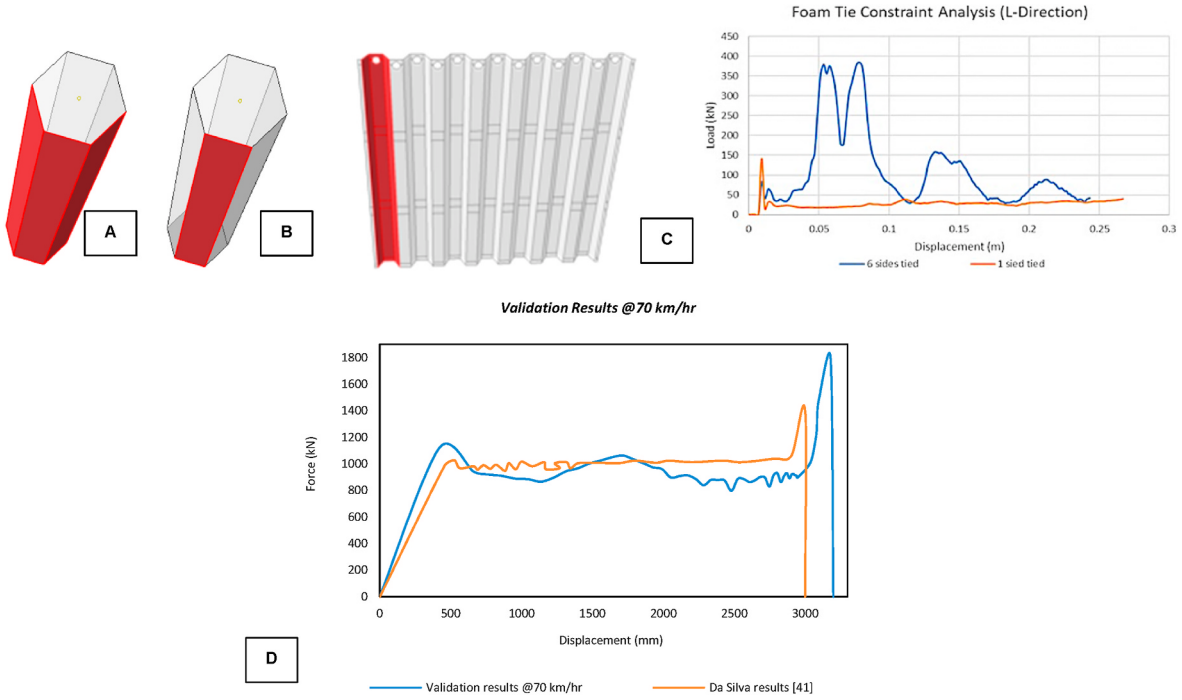


Fig. 7. A) Surfaces of foam selected for tie constraint analysis, 6 sides and one side, B) Tie constrained surfaces on the sheet, C) Tie constraint analysis on 6 sides and 1 side of foam in L-direction impact and D) Validation results, 70 km/h impact in L-direction.

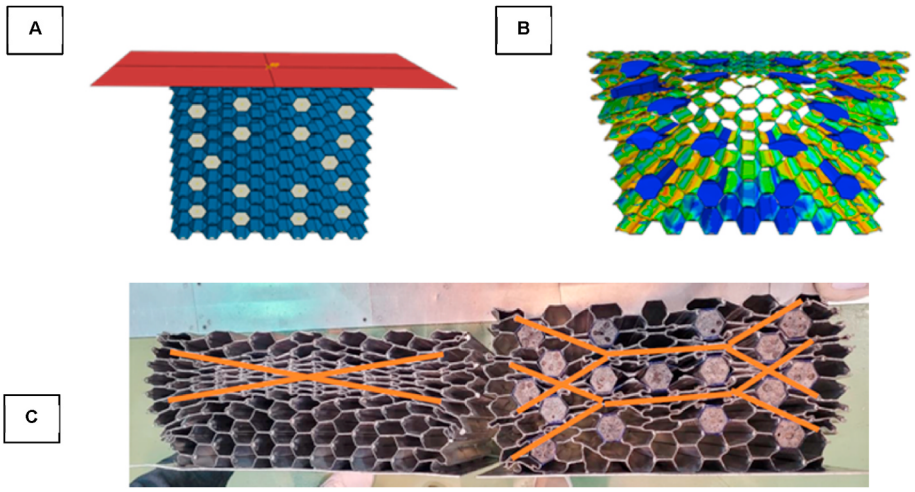


Fig. 8. A) Foam-filled honeycomb in L-direction impact, B) FEA and C) Experimental deformations.

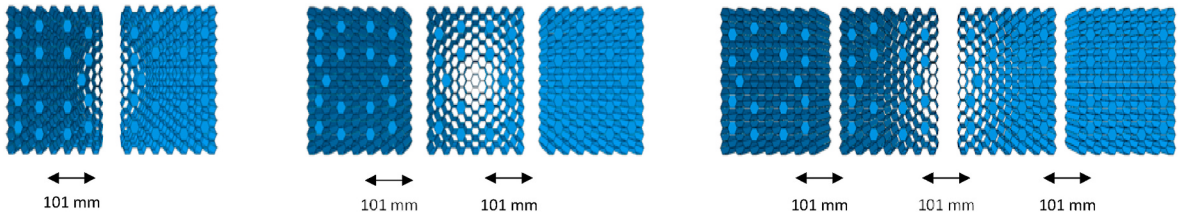


Fig. 9. Scenarios II, III-A, III-B in T-direction impact with 1 mm thick corrugated sheets.

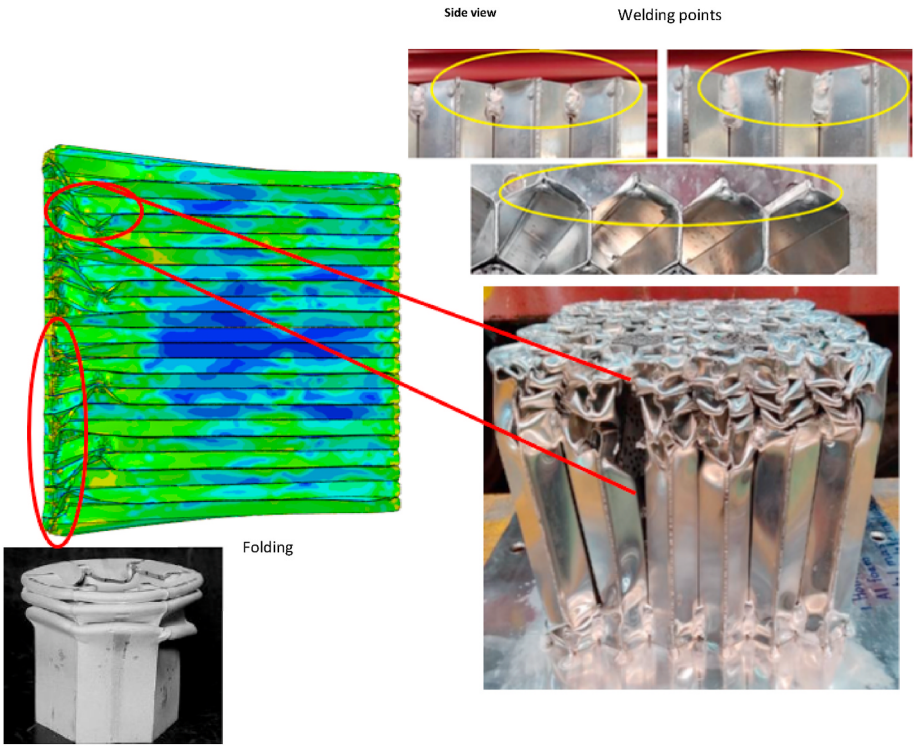


Fig. 10. Comparison of simulated (calibrated model) and experimental deformations, T-direction impact.

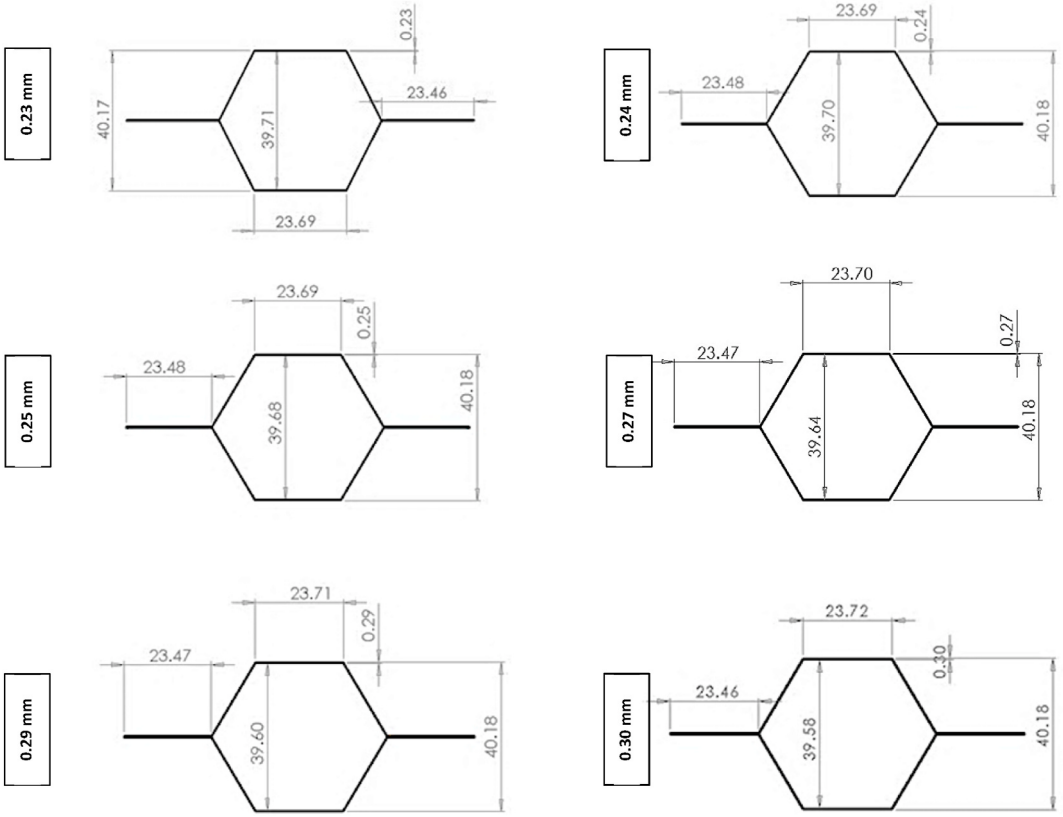


Fig. 11. The geometry of the hexagonal cell with 0.23 mm, 0.24 mm, 0.25 mm, 0.27 mm, 0.29 mm, and 0.30 mm corrugated sheet thickness.

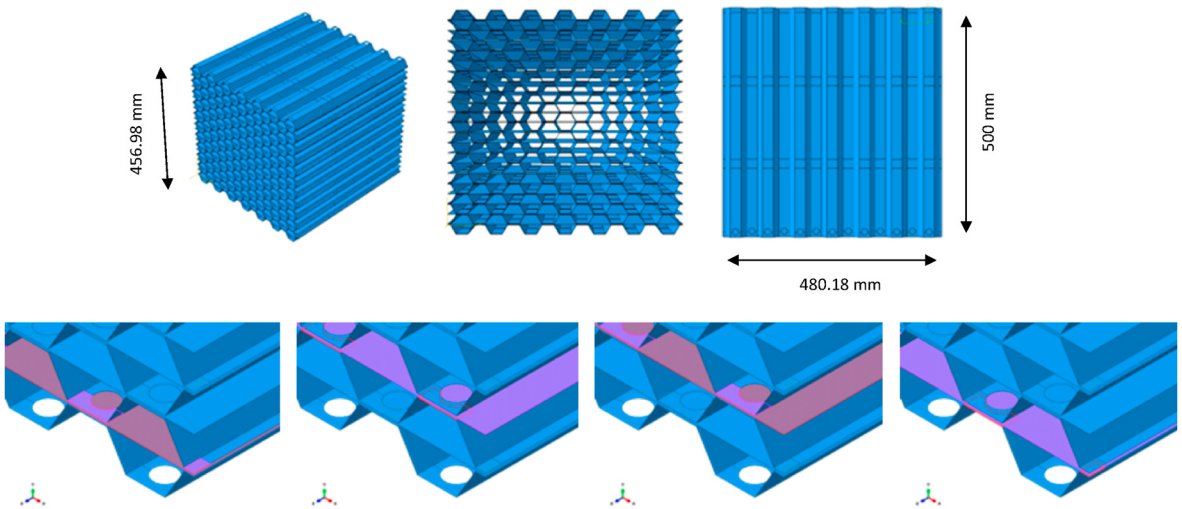


Fig. 12. Model of the reinforced honeycomb structure (top), successive master/slave in red (bottom). (For interpretation of the references to colour in this figure legend, the reader is referred to the Web version of this article.)

3. Numerical approach

3.1. Corrugated sheet and stiffener material model

Following the authors' experimental studies (Nicoud et al., 2023; Valente, 2021), the aluminium corrugated sheets were modelled with Johnson-Cook (J-C) flow stress and fracture model. The J-C flow stress model is defined as:

$$\sigma = (A + B\varepsilon^n)(1 + C ln\dot{\varepsilon}^*)(1 - T^{*m}) \quad (1)$$

where $T^* = \frac{T - T_{ref}}{T_m - T_{ref}}$, $\dot{\varepsilon}^* = \frac{\dot{\varepsilon}}{\dot{\varepsilon}_{ref}}$.

A, B, n parameters are calculated as follows $\sigma = (A + B\varepsilon^n) \Leftrightarrow \ln(\sigma - A) = n \ln(\varepsilon) + \ln(B)$. The J-C fracture model is defined as:

$$\varepsilon_f = \left[D_1 + D_2\, exp\left(D_3 \frac{\sigma_m}{\sigma_{eq}}\right)\right]\left[1 + D_4\, ln\left(\dot{\varepsilon}_p^*\right)\right][1 + D_5 T^*] \quad (2)$$

Eq. (2) can be modified by neglecting the effects of temperature and strain rate and using the stress triaxiality effect term which can be written as follows,

$\varepsilon_f = D_1 + D_2\, exp(D_3\sigma^*)$. The values of C, m, D_4 and D_5 were deter-

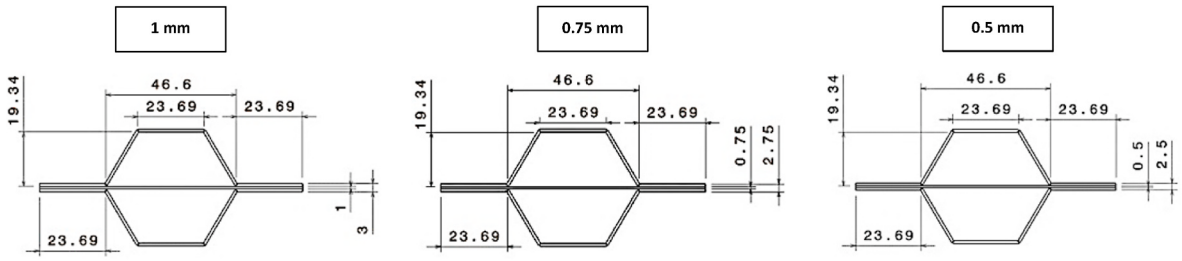


Fig. 13. Hexagonal cell geometry with 1 mm sheet thickness and 1 mm, 0.75 mm, 0.5 mm stiffener thickness.

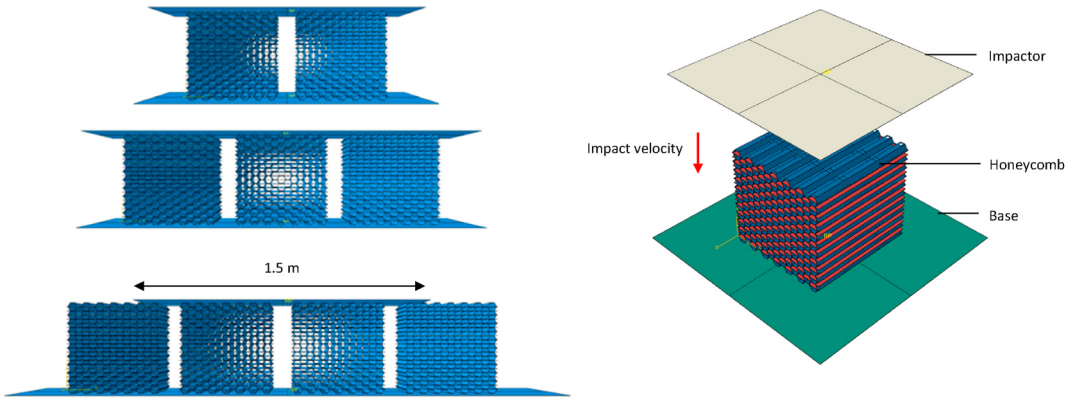


Fig. 14. FEM model for each scenario with stiffener-reinforced designs.

Table 4
Results for foam-filled honeycomb designs in T-direction impact for each scenario.

Scenario/sheet thickness	*Mass (Kg)*	*MD (mm)*	*PCF (kN)*	*MCF (kN)*	*AE (kJ)*	*SEA (kJ/kg)*	*CFE (%)*	*PA (g)*	*MA (g)*
I/1 mm	23.3	14	322	186	37.8	1.5	57.7	21.9	21.6
II/1 mm	46.7	16	268	163	77.5	0.7	60.9	18.2	17.8
III-A/1 mm	69.7	43	465	185	13.1	0.2	39.8	31.6	13.5
III-B/1 mm	92.9	41	444	175	13.4	0.2	39.8	30.2	12.1
III-A/0.23 mm	26.2	251	835	436	141.3	5.4	52.3	56.7	29.1
III-B/0.23 mm	34.9	260	830	85	136.2	2.7	54.4	56.4	32.7

mined in (Nicoud et al., 2023; Valente, 2021) (see Table 1).

3.2. Aluminium foam model

Aluminium foam compression tests have been established as a material model as explained in (Valente et al., 2023; Nicoud et al., 2023; Valente, 2021; Gibson, 2003; Fleck, 2016; Nicoud, 2022). Key values, including densification strain, foam Young's modulus, and plateau stress, are detailed in Table 2. The Crushable Foam Plasticity Isotropic Hardening model in ABAQUS has been specifically designed for the compressive behaviour of metallic foam which integrates the isotropic hardening model for an effective analysis (see Fig. 2) (see Table 3).

3.3. Empty honeycomb (unreinforced design) geometry

The honeycomb geometry uses aluminium corrugated sheets constrained together to simulate welded sheets, each representing half a hexagonal cell. Using the mid-plane method, half-hex cells and stiffeners are modelled with sheets extruded by 500 mm. A trigger mechanism is integrated at one end of the corrugated sheet, featuring a hole with a 7 mm radius (see Fig. 1). The assembly includes corrugated sheets, an impactor, a base, foam fillings, and stiffeners if present. SolidWorks was used to model shell geometry based on the authors' optimisation guidelines with 18 filled cells in the honeycomb core (Valente, 2021).

3.4. Crash scenarios

The defined scenarios involve various energies and crash box configurations. Scenario I, with 36.25 kJ energy, equivalent to one-fourth of the total KE of a 1500 kg vehicle at 50 km/h, used an 800 × 800 mm impactor at 6.95 m/s. Scenario II featured two crash boxes, a larger 1400 × 800 mm impactor, half the total KE (74.5 kJ), and a speed of 9.83 m/s. Scenario III-A introduced three crash boxes, maintaining honeycomb dimensions, with total applied kinetic energy at 13.89 m/s. Scenario III-B expanded to four crash boxes, using the same energy and a larger 1500 × 800 mm impactor, not entirely overlapping side crash boxes (see Fig. 3). The separation between each crash box in scenarios II, III-A, and III-B was 101 mm.

3.5. Constraints, interactions, and boundary conditions

The corrugated sheets assembly uses tie-constrained surfaces for welding points (see Fig. 4), foam fillers, and stiffeners. Additional tie constraints secure the assembly (slave) to the base plate (master), preventing relative movement. General contact with "hard" contact for normal behaviour is implemented between the structure and the impactor to prevent penetration. This contact is also applied between corrugated sheets and within each sheet. The first boundary condition fixes all degrees of freedom (DOF) for the base plate. The second and third conditions on the impactor constrain all DOF except in the impact

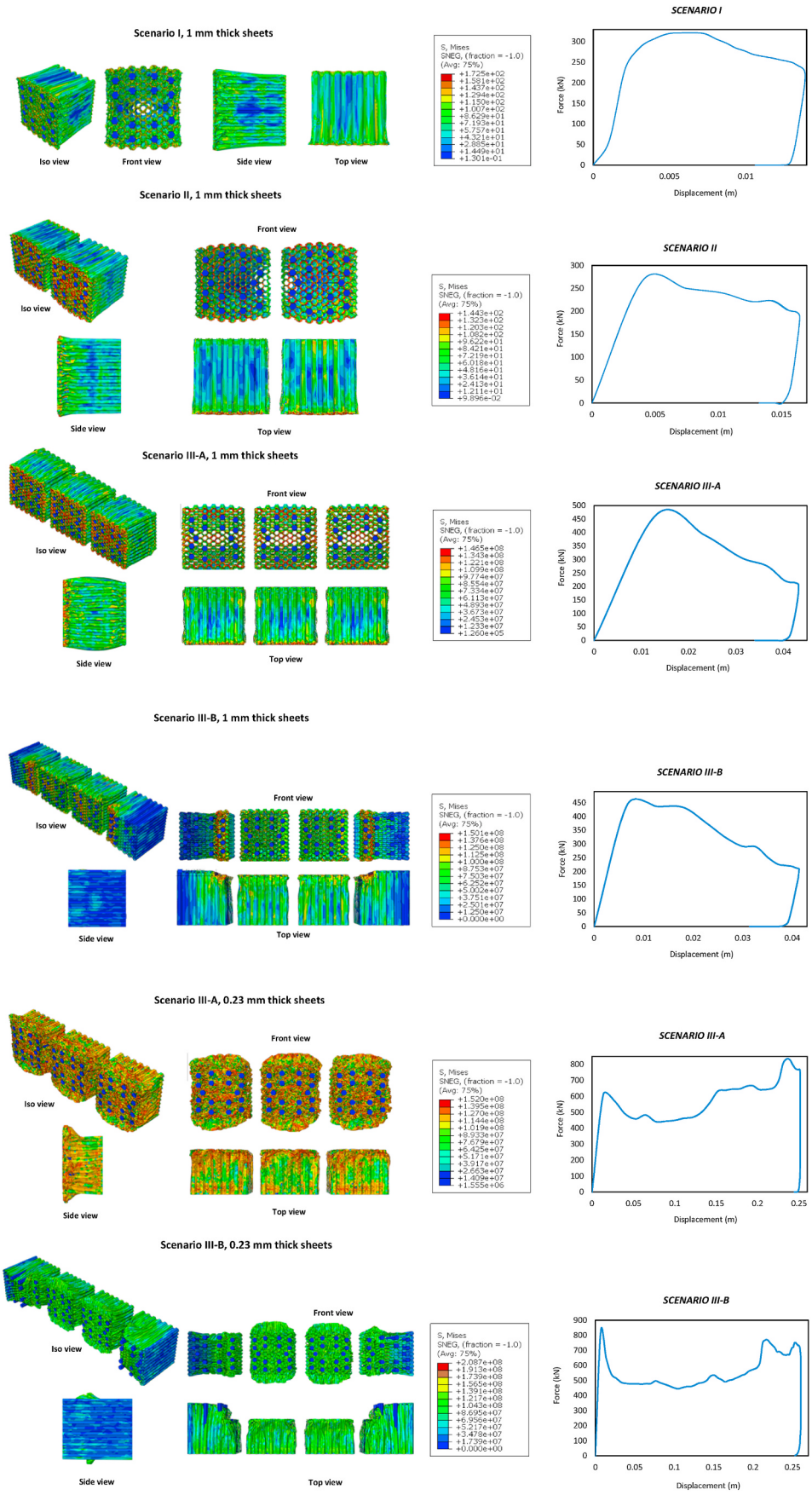


Fig. 15. Von-Mises stress distributions in the final crushing stage (left) and FD diagrams (right), all scenarios in T-direction impact, 0.23 mm and 1 mm thick sheets filled with aluminium foam.

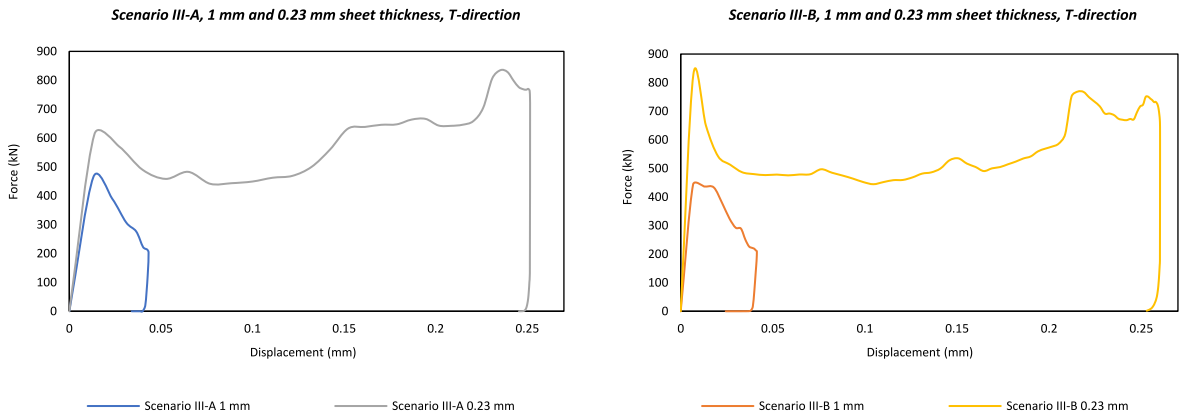


Fig. 16. Scenario III-A and III-B, FD diagrams, 1 mm and 0.23 mm sheet thickness, T-direction.

Table 5
Results for foam-filled honeycomb with 1 mm sheet thickness in L-direction.

Scenario	*Mass (Kg)*	*MD (mm)*	*PCF (kN)*	*MCF (kN)*	*AE (kJ)*	*SEA (kJ/kg)*	*CFE (%)*	*PA (g)*	*MA (g)*
I	23.2	382	172	41	31.8	1.4	23.8	11.7	2.8
II	46.5	397	569	112	42.2	0.9	19.7	38.7	7.6
III-A	69.7	373	248	139	53.4	0.8	56.0	16.9	9.4
III-B	92.9	298	210	164	53.5	0.5	78.1	14.3	11.1

direction, setting a predefined initial velocity.

3.6. FE model development

Incorporated behind crash boxes, a 3D analytical rigid shell base prevents material overflow during the densification phase. Analytical rigid surfaces are described as analytical functions as their deformation is negligible, reducing computational time. For corrugated sheets, partitioning defines welding points and assigns mass at the centre of the rigid impactor. The corrugated sheets were modelled as shells and used a middle surface offset to eliminate errors regarding the distance between stacked sheets. Mass scaling, crucial for dynamic explicit simulations, ensures equal stable time increments (1μsec) for all elements. S4R shell elements with hourglass control and element deletion enabled model corrugated sheets and stiffeners, while C3D8R solid elements represent aluminium foam. Mesh convergence analysis determined an optimal size of 4.1 mm for corrugated sheets. S4R elements, selected for their six DOF, efficiently simulate collapse mechanisms like folding, allowing sheet thickness definition, computational efficiency, shear locking resistance, and the incorporation of transverse shear deformation. High-performance computing was facilitated to perform calculations due to the high element count. An example of the FE model for scenario-II simulation is shown in Fig. 5.

3.7. Foam-filled honeycomb designs and validation model

The validation model drew insights from previous experimental studies, to establish suitable constraints and boundary conditions, and determine an optimal mesh size ensuring accurate results. The validation was done with the foam-filled honeycomb subjected to an impact in the L-direction, the corrugated sheet thickness is 1 mm and the dimensions are given in Fig. 6. S4R shell elements were employed for the aluminium corrugated sheets. The aluminium foam was modelled with C3D8R solid elements and incorporated a hard contact to prevent unrealistic penetration and a tangential contact with a coefficient of friction of 0.2 to simulate sheet-foam interactions, the foam being the slave and the honeycomb the master.

A mesh sensitivity analysis on the corrugated sheets and the foam sought an optimal balance between accuracy and computation time, focusing on the relationship between corrugated sheets and foam mesh sizes in L-direction impact. The analysis was made with the foam solid part tied to the sheets at only one side face as shown in Fig. 7. Initially, the foam mesh size mirrored that of the sheets, however, this revealed a considerably higher peak stiffness than reality. The foam mesh size exerted a more significant influence than the sheet mesh size. Increasing the sheet mesh size while keeping the same foam mesh size resulted in increased peak stiffness. Finally, a mesh size of 4.1 mm for the sheet and 25 mm for the foam was chosen as it led to the best results. As observed in Fig. 8, tying the foam on all six sides to the sheet introduced excessive stiffness, while tying one side yielded suitable results. A robust correlation with less than 20% error is observed between experimental results [33] and our simulation with an axial impact (T-direction) done with a 1500 kg impactor launched at 70 km/h. Deformation patterns for the L-direction differ for empty and foam-filled honeycomb structures are presented in Fig. 8. The deformations achieved in the calibrated simulation also align closely with the experimentally observed deformations in L-direction impacts.

Numerical setups in L and T-direction are similar and scenarios in T-direction impact are presented in Fig. 9. The numerical deformations and Von Mises (VM) stress distribution at the final stage of an axial impact subjected to scenario I are shown next to the experiment under the same impact set-up in Fig. 10. The model uses the parameters from the validated model and the effects of the different characteristics are observed (welding points, trigger mechanism, folding).

3.8. Honeycomb designs with various corrugated sheet thicknesses

Unreinforced honeycomb designs in T-direction impact (0.23 mm–0.30 mm sheet thickness) were explored for crashworthiness emphasising minimal mass and design enhancements while MA $<$ 20g. The honeycomb dimensions align with prior foam-filled specimens, maintaining consistency with the FE model. The initial design, featuring 0.23 mm thick sheets, comprises 22 corrugated aluminium sheets forming 11 hexagonal rows (see Fig. 11). The geometry of the assembly closely matches with a sheet thickness reduction only on the inner side of the hexagon while maintaining outer dimensions. Geometry adjustments were executed in SolidWorks and MATLAB with a concentration on scenarios III-A and III-B, addressing high energy absorption

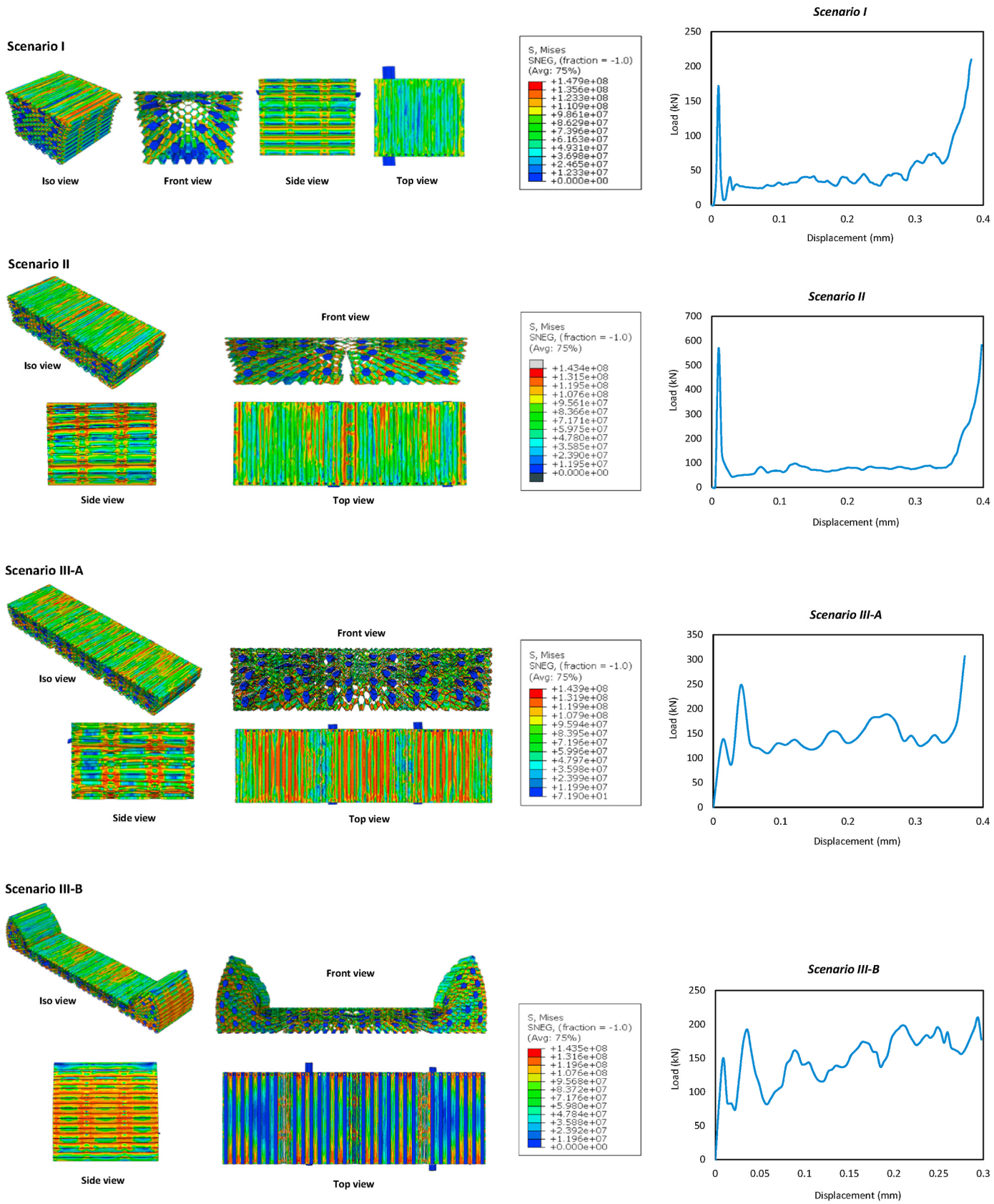


Fig. 17. Von-Mises stress distributions in the final crushing stage (left) and FD diagrams (right), all scenarios in L-direction impact, 1 mm thick sheets with aluminium foam fillers.

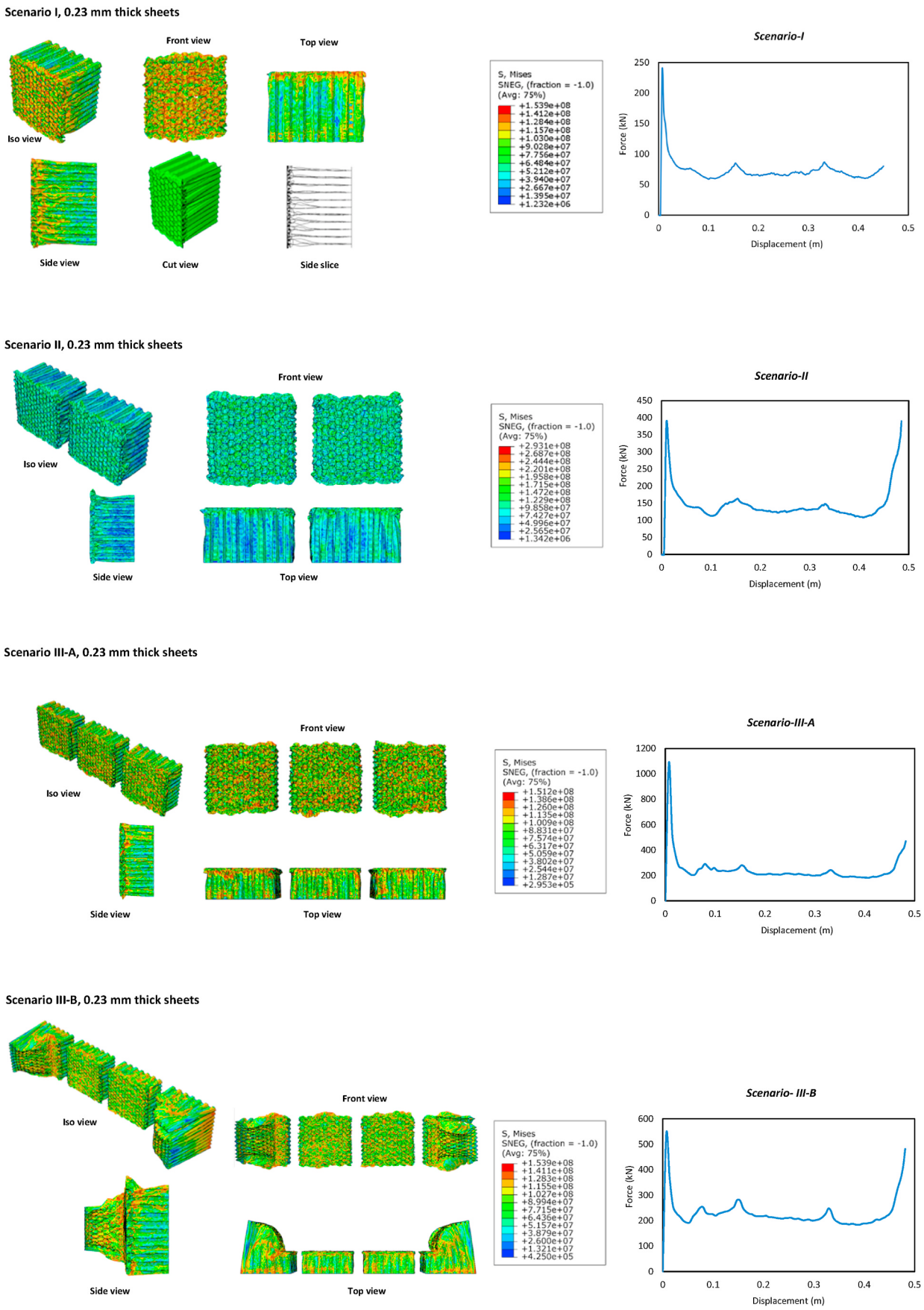


Fig. 18. Von-Mises stress distributions in intermediate crushing state (left) and FD diagrams (right), all scenarios in T-direction impact, 0.23 mm thick sheets.

Table 6
Crashworthiness indicators for various sheet thicknesses and scenarios.

Scenario/sheet thickness	Mass (kg)	MD (mm)	PCF (kN)	MCF (kN)	AE (kJ)	SEA (kJ/kg)	CFE (%)	PA (g)	MA (g)
I/0.23 mm	4.3	450	235	71	32.7	7.5	30.3	16.0	4.9
II/0.23 mm	8.7	485	382	135	63.2	7.3	35.3	26.0	9.2
III-A/0.23 mm	13.0	482	1084	228	110.4	8.5	21.1	73.7	15.5
III-B/0.23 mm	17.3	481	539	218	104.1	6.0	40.5	36.7	14.8
III-A/0.24 mm	13.6	490	1108	221	108.6	8.0	19.9	75.3	15.0
III-B/0.24 mm	18.0	486	488	215	104.1	5.8	44.1	33.2	14.6
III-A/0.25 mm	14.1	490	1155	231	116.1	8.2	20.0	78.5	15.7
III-B/0.25 mm	18.8	488	460	208	102.0	5.4	45.2	31.3	14.1
III-A/0.27 mm	15.3	464	1248	254	125.2	8.2	20.4	84.9	17.3
III-B/0.27 mm	20.3	475	551	239	117.6	5.8	43.3	37.4	16.2
III-A/0.29 mm	16.4	484	1343	270	137.2	8.4	20.1	91.3	18.4
III-B/0.29 mm	21.8	469	610	259	123.2	5.6	42.5	41.5	17.6
III-A/0.30 mm	16.9	480	1389	283	144.2	8.5	20.4	94.4	20.4

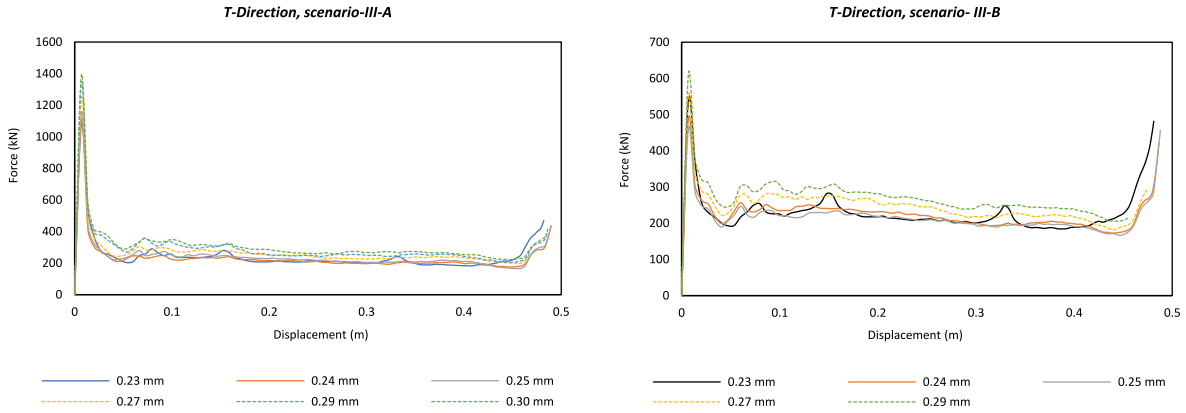


Fig. 19. FD diagrams for scenarios I and II for 0.23 mm sheet thickness and scenarios III-A and III-B with sheet thickness ranging from 0.23 mm to 0.30 mm.

requirements and real-life applicability.

3.9. Stiffener reinforced honeycomb designs

Reinforced honeycomb designs in L-direction impact incorporated aluminium plates as stiffeners between corrugated sheets (see Fig. 12), exploring lightweight crashworthy configurations with MA < 20g. The honeycomb, measuring 480 × 457 × 500 mm^3, employed a similar FE model to previous cases. Stiffener thicknesses of 1 mm, 0.75 mm, and 0.5 mm were tested, maintaining a constant 1 mm thickness for the corrugated sheets. The assembly integrated 20 stiffeners welded to corrugated sheets with trigger mechanisms on sheets only for minimal manufacturing changes. Geometric details for one honeycomb cell with a stiffener are in Figs. 13 and 14. Tie constraints were applied at welding points, and optimal results were achieved when alternating master and slave roles between stiffener and sheet for each tie. General contact with a friction coefficient of 0.2 was used to model interactions between sheets and stiffeners.

4. Results and discussion

4.1. Expectations towards the crashworthiness results

Design objectives aimed to absorb 145 kJ of kinetic energy from a 1500 kg vehicle at 50 km/h with an acceleration of less than 20g, complying with European automotive safety standards. Newton's law indicates a maximum necessary MCF of about 300 kN for controlled deceleration. Calculations indicated a minimum end displacement of 0.5 m and the maximum required crushing length of the structure is 0.5 m. The study targeted a structure with an MCF of 300 kN during impact, minimising material needs and structural length.

4.2. Foam-filled honeycomb with 1 mm and 0.23 mm corrugated sheet thicknesses - T-direction impact

Crashworthiness parameters for two honeycomb designs (1 mm or 0.23 mm sheet thickness) are summarised in Table 4. Scenario I (25% total KE, 36.25 kJ) exhibit minimal deformation (14 mm displacement), with no steep peak force or densification zone, indicating an excessively stiff structure. Scenario II (50% total KE, 72.5 kJ) shows negligible deformation (16 mm displacement), lacking a clear densification zone and no steep peak suggesting insufficient AE. Scenario III-A (full impact energy, 145 kJ) displays minimal deformation (40 mm displacement) for the 1 mm thickness design, highlighting its high rigidity. Scenario III-B yields similar results as the 0.23 mm thickness design in T-direction impact (Scenarios III-A and III-B) shows increased AE and SEA with larger displacement, featuring a distinct pattern of initial PCF, plateau, and densification. Despite exceeding the 20g limit, the 0.23 mm thickness is preferred. In summary, thinner sheets enhance AE, while additional crash boxes increase stiffness, resulting in higher accelerations. Future optimisation involving sheet thickness within the 0.23–1 mm range is suggested for lower acceleration and higher SEA (see Figs. 15 and 16).

4.3. Foam-filled honeycomb with 1 mm corrugated sheet thickness, L-direction impact

Crashworthiness parameters in L-direction analysis with 1 mm sheet thickness are summarised in Table 5. Scenario I (36.25 kJ) yield a PA of 11.7g, MA of 2.8g, CFE of 23.8%, and low AE (31.8 kJ). Scenario II (72.5 kJ) shows higher PA (38.7g), MA (7.6g), and very low AE (42.2 kJ). Scenario III-A (145 kJ) exhibits PA of 16.9g, MA of 9.4g, a very low AE (53.4 kJ), and a relatively good CFE (56%). However, scenario III-B (145 kJ) absorbs only 53.5 kJ, indicating this foam-filled honeycomb

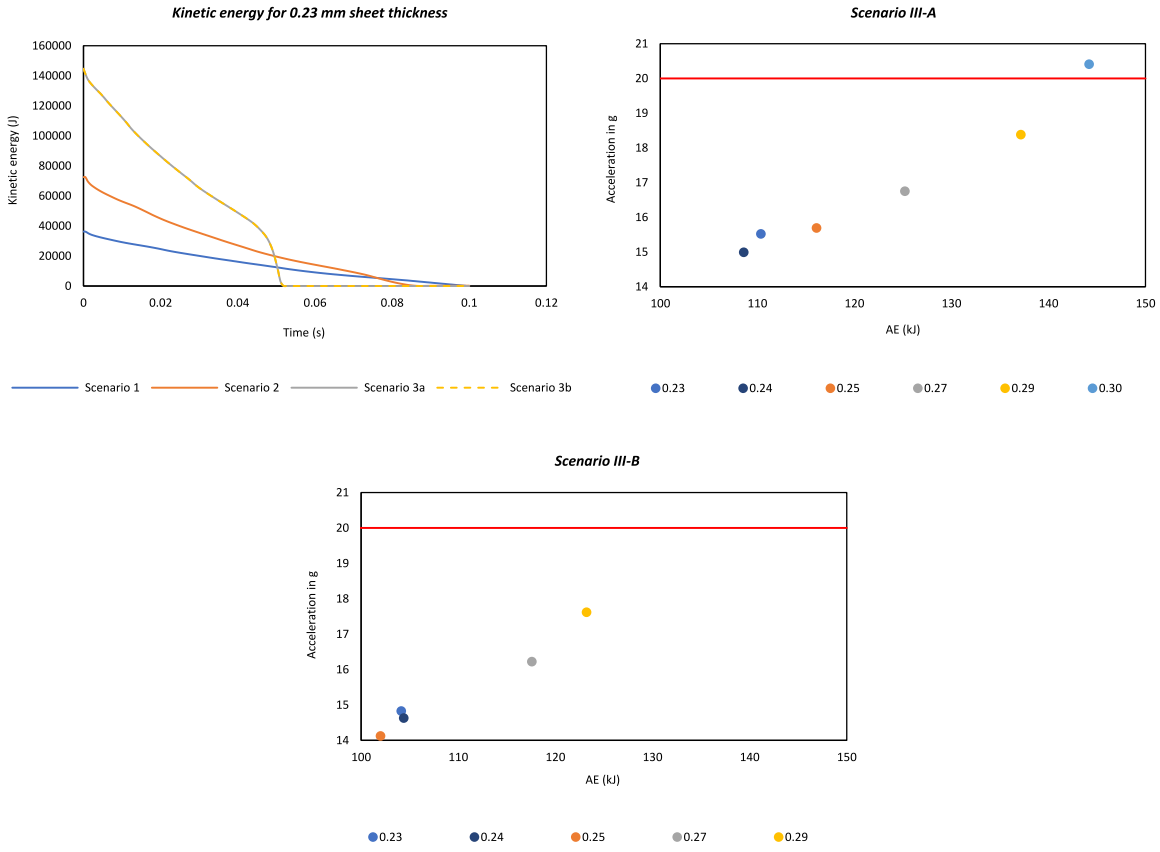


Fig. 20. KE evolution, comparison of AE and MA for various thicknesses (mm) and scenarios.

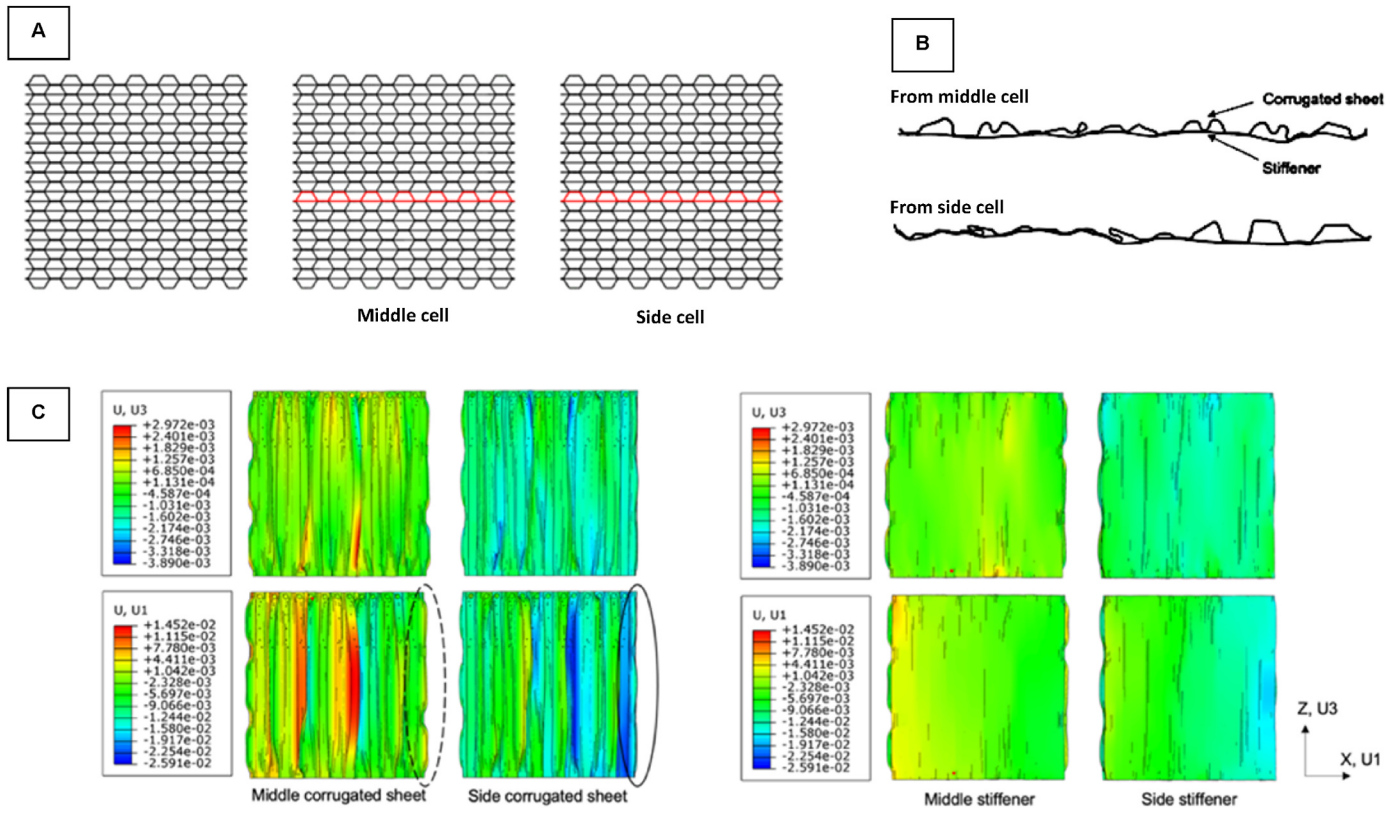


Fig. 21. A) Selected stiffeners and corrugated sheet in red, scenario III-A, profile view. B) Section view of the selected stiffeners and corrugated sheets in plane 1, and C) In-plane displacements U1 and U3 (in m) for the middle and side cells corrugated sheets and stiffeners. (For interpretation of the references to colour in this figure legend, the reader is referred to the Web version of this article.)

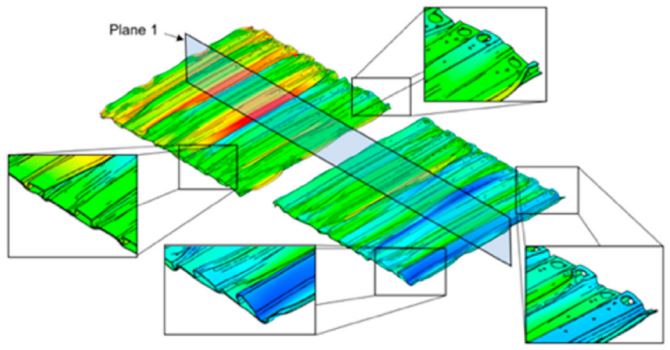


Fig. 22. Isometric view, U1 displacement on corrugated sheets and stiffeners, middle cell on the left, side cell on the right.

design failed to absorb the total applied kinetic energy in all scenarios in the L-direction despite low PA and MA. Our results indicate that increased crash boxes enhance CFE up to 78.1% in scenario III-B (see Fig. 17).

4.4. Honeycomb designs with various corrugated sheet thicknesses, T-direction impact

In this section, results for honeycomb designs with sheet thicknesses between 0.23 mm and 0.30 mm are presented. Stress distribution during intermediate collapse states, the structure being completely crushed at the final state, and force-displacement diagrams for 0.23 mm sheets (design 1) and scenarios III-A and III-B for other thicknesses are provided. Comparative diagrams for AE and MA of different designs are included. Deformations for design 1 show welding deboning occurring away from the crash front. The section view reveals material folding near and away from the crash front, while the right-wired view illustrates the expanded separation of corrugated sheets. For design 1, stress distribution at an intermediate collapse state reveals consistent crushing behaviour, higher stress values near the crash front (150 MPa), and similar patterns for scenarios I to III-A, attributed to the development of energy-absorbing mechanisms, such as material folding. In scenario III-B, the collapse pattern of simple design 1 deviates due to the impactor not completely overlapping the four crash boxes, resulting in distinct collapse patterns between the central and side boxes. While the central two boxes collapse similarly in all scenarios, the side boxes exhibit visible folding and intense bending. This bending initiates stress concentration near the base, causing increasing resistance force on the impactor and potentially influencing crashworthiness parameters. The incomplete overlap of the impactor leads to a smoother transition from PCF to the plateau region. Fig. 18 displays force-displacement diagrams for all scenarios, following the typical curve shape of aluminium crushing behaviour. Scenarios II, III-A, and III-B exhibit a knee, marking the onset of densification. PCF values align closely, increasing with greater sheet thickness, signifying enhanced structure resistance. This trend extends to the plateau region, where higher sheet thickness correlates with increased load values, leading to greater AE. Kinetic energy versus time indicates earlier densification for higher KE impacts. Crashworthiness parameters indicate highlighted lightweight structures with SEA ranging from 6 kJ/kg (scenario III-B) to 8.50 kJ/kg (scenario III-A). PCF, AE, and CFE show variations with applied energy and additional crash boxes. The PCF is higher in scenario III-A than III-B, due to the bending collapse of side box structures. AE consistently falls short of applied energy, especially in scenarios III-A and III-B indicating the inefficacy of this design to absorb the initial KE. CFE increases with applied energy and additional crash boxes. PA exceeds 20g in scenarios II, III-A, and III-B. However, MA stays below 20g for all scenarios, with

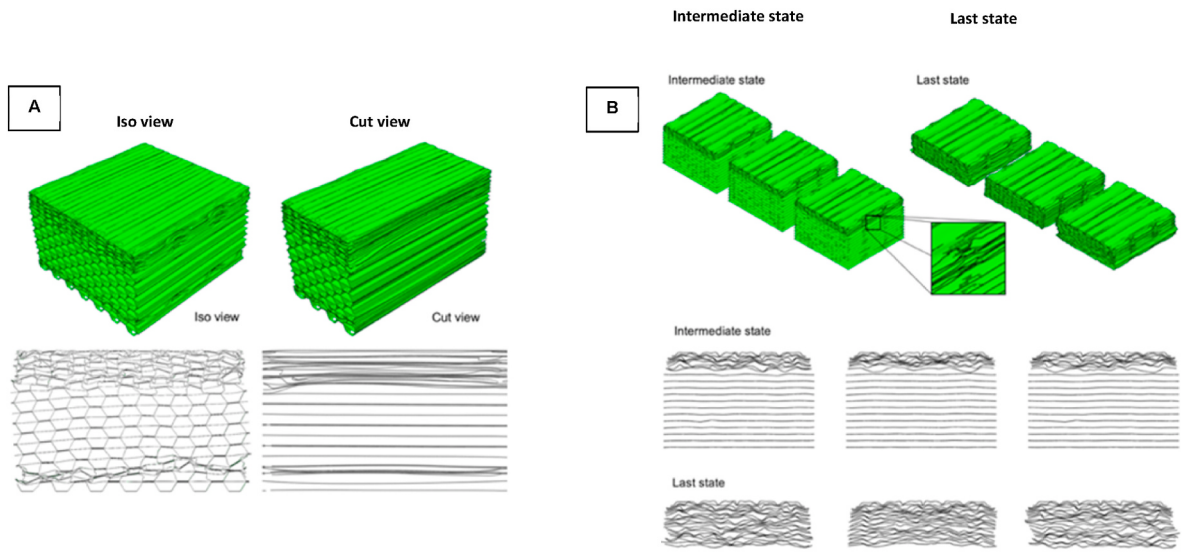


Fig. 23. A) Deformations of reinforced honeycomb for scenario I, full assembly on the top left, cut on the top right, slices at the bottom, and B) Deformations of stiffeners reinforcements for scenario III-A, stiffeners only assembly on the top left, cut on the top right, slices at the bottom.

15.52g being the highest value in scenario III-A and 4.87g being the lowest in scenario I. Table 6 summarises crashworthiness metrics for other unreinforced honeycomb designs in scenarios III-A and III-B, focusing on sheet thickness variations (0.24 mm–0.30 mm). Mass increases with thicker sheets, peaking at 21.83 kg for 0.29 mm thickness in scenario III-B. Optimal performance is seen with 0.29 mm thickness in scenario III-A, yielding 137.16 kJ AE with SEA around 8.30 kJ/kg and CFE at 20%, while scenario III-B exhibits SEA at 5.60 kJ/kg and a CFE at 43%. MCF and PCF generally increase with sheet thickness, while SEA and CFE maintain consistent values. Comparative diagrams illustrate AE and acceleration for each sheet thickness in scenarios III-A and III-B (see Fig. 19). The 0.29 mm thickness is optimal, balancing high AE (around 140 kJ) while keeping acceleration below 20g, although, in scenario III-B, AE values are not as high as in III-A due to the bending response (see Fig. 20).

4.5. Stiffener reinforced honeycomb with various stiffener thicknesses and 1 mm corrugated sheet thickness, L-direction impact

Reinforcements improve reaction force levels, aiding impactor energy absorption without entering the densification zone. Reinforced hexagonal honeycombs outperform traditional ones in absorbed energy with the same PCF. Aluminium plates between each corrugated sheet initially have a 1-mm thickness as shown in Figs. 21–24. Varying thickness to assess impact on force levels is of interest as shown in Fig. 25. Foam fillers in the L-direction provide no enhancement; empty specimens exhibit superior SEA. Table 7 presents crashworthiness results for 1 mm, 0.75 mm, and 0.5 mm stiffener thickness. Simulations show increased force levels for stiffener-reinforced honeycombs compared to empty designs. With 1 mm sheet thickness, III-A and III-B reach 350–550 kN, exceeding foam-filled and stiffener variants in I and II. Plastic deformation waves in I and II initiate from top and bottom, moving towards the centre with greater emphasis on the top crash front, as shown in Fig. 23. L-direction impacts with stiffeners exhibit oscillations differing from T-direction impacts where the inner cells deform completely because of the constraint by the neighbouring cells, as found previously in this paper and according to the previously achieved results (Aktay et al., 2008; Yamashita and Gotoh, 2005). The middle section has less deformation, and studying varied stiffener properties in that region would be of interest. Honeycomb deformation primarily occurs in the impact direction, with stiffeners unaffected by buckling due to tensile stress as sheets spread. Localised elastic buckling absorbs energy reversibly. As critical stress shifts from elastic to plastic phases, the honeycomb undergoes plastic collapse, maintaining relatively constant compressive stress. Walls plastically collapse, foils contact, and stack, with a consistent plateau stress observed, particularly significant for engineering applications. The structural load level and AE depend significantly on stiffener thickness. Crash boxes exhibit consistent behaviour, with stress values ranging between 140 MPa and 150 MPa and AE being nearly equal to initial impact energy. FD diagrams (Figs. 24 and 25) with 1 mm stiffeners show peak loads, a plateau, and no densification, with comparable PCF in III-A and III-B and greater SEA in III-A. In III-A and III-B, reducing thickness induces modest force rises, but acceleration increases, exceeding the 20g target. For III-A, it progressed from 27.6g to 29.4g with 0.5 mm stiffeners. MA increased from 28g to 29.6g in III-B with 0.5 mm. Compared to the design with 1 mm stiffener thickness, 0.75 mm thick stiffeners exhibit heightened AE and SEA. The stiffener thicknesses of 1 mm and 0.75 mm prevent total collapse but induce high forces, while 0.5 mm stiffeners cause a large final densification zone, changing structural stiffness. Results suggest a threshold in stiffener thickness marking the onset of densification, compromising energy absorption efficiency. III-A and III-B exhibit slight acceleration increases with reduced thickness. CFE remains consistent for III-A around 35% for all reinforced designs, varying for III-B from 57.9% for 0.75 mm to 36.6% for 1 mm stiffeners. Fig. 26 displays KE-time diagrams, showing consistent decline rates for scenarios III-A and III-B across all designs. III-A and III-B absorb the initial impact KE in less time compared to I and II, explained by the strain rate effect modelled by the Johnson-Cook material law, accounting for differences in impact velocity.

5. Conclusions

This research studied crashworthiness performance by enhancing energy absorption of honeycomb energy absorbers in T and L-direction impact, targeting MA<20g. Unreinforced honeycomb designs (0.23–0.29 mm wall thickness) achieved MA<20g with high SEA and CFE. The 0.29 mm sheet thickness unreinforced design excels, displaying MA of 18.4 g and AE of 137.2 kJ (145 kJ initial KE). Thinner sheets yield lower acceleration, while the densification phase induces lower AE. In T-direction impacts, adding aluminium foam fillers with the 0.23 mm sheet thickness design increases absorbed energy but raise stiffness, elevating accelerations. Foam-filled designs with 1 mm sheet thickness exhibit reduced absorbed energy due to heightened stiffness in T-

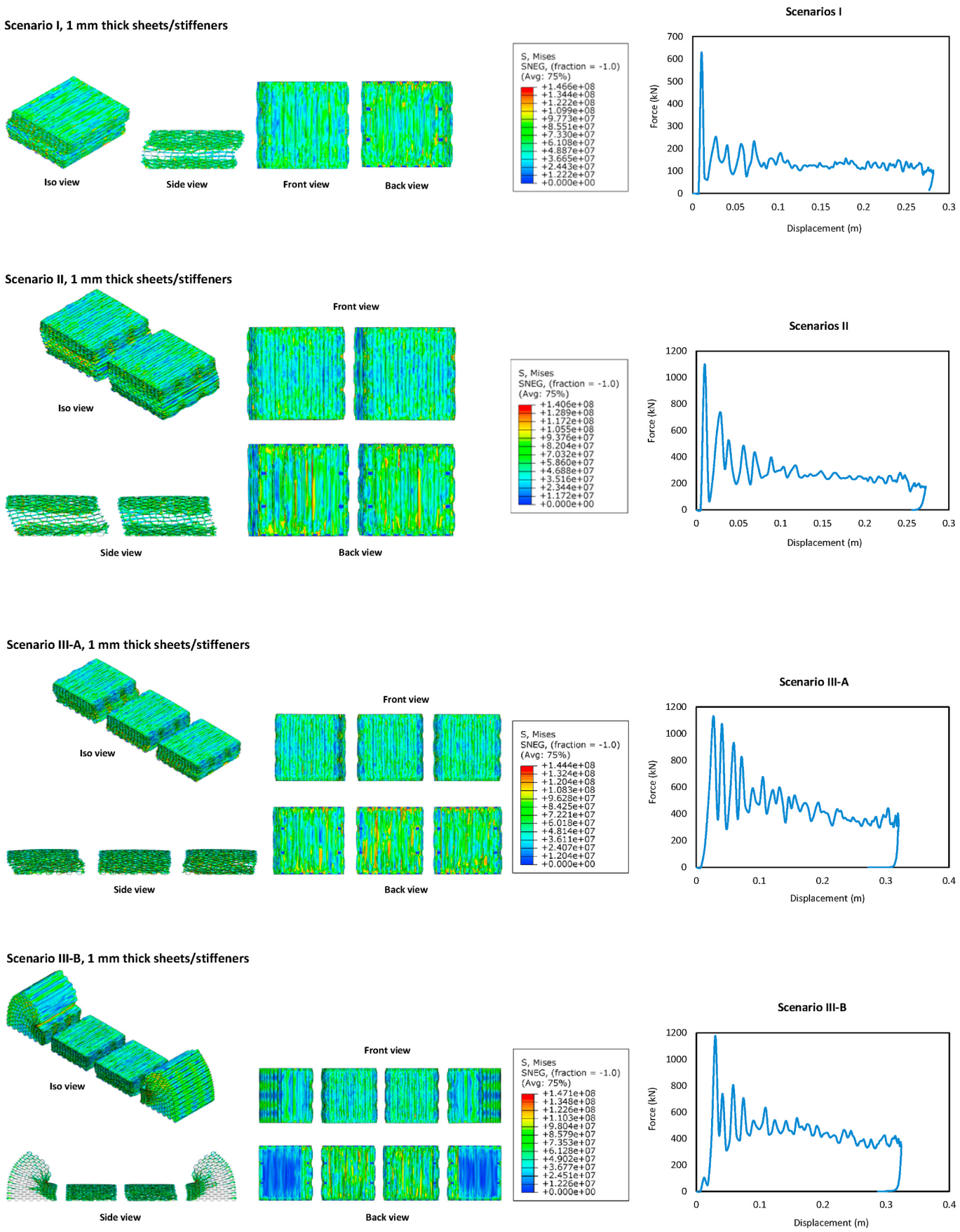


Fig. 24. Von-Mises stress distributions in final crushing state (left) and FD diagrams (right), all scenarios in L-direction impact, 1 mm thick sheets and stiffeners.

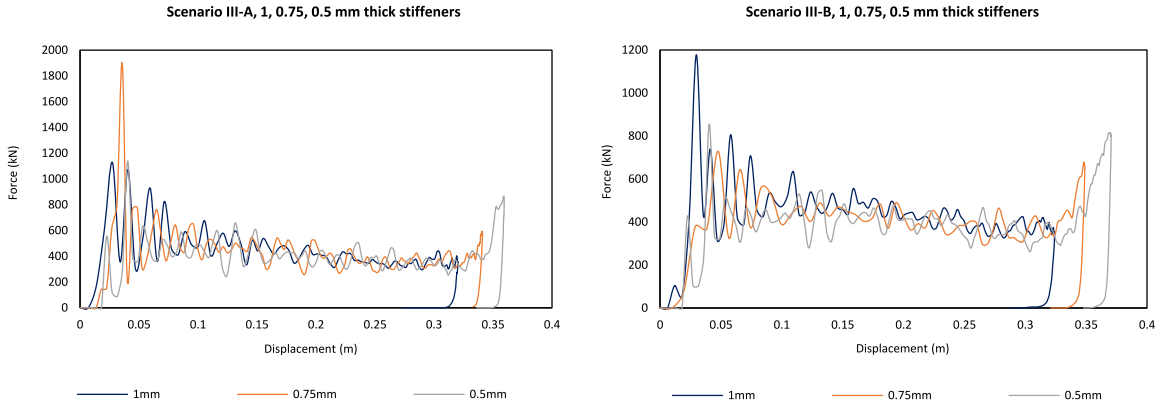


Fig. 25. Force displacement diagrams with various scenarios and thicknesses for stiffeners, L-direction impact.

Table 7
Crashworthiness results with each scenario for 0.5, 0.75, and 1-mm thick stiffener-reinforced honeycomb designs.

Scenario/stiffener thickness	Mass (kg)	MD (mm)	PCF (kN)	MCF (kN)	AE (kJ)	SEA (kJ/kg)	CFE (%)	PA (g)	MA (g)
I/1 mm	32.5	0.28	630	124	37.8	1.2	19.6	42.8	8.4
II/1 mm	65	0.27	1100	245	77.5	1.2	22.3	74.8	16.6
III-A/1 mm	97.5	0.32	1128	407	143.6	1.5	36.1	76.7	27.7
III-B/1 mm	130	0.32	1128	413	141.4	1.1	36.6	76.7	28.1
III-A/0.75 mm	87.2	0.34	1896	418	144.3	1.7	37.1	128.9	28.4
III-B/0.75 mm	116.3	0.35	729	418	139.2	1.2	57.9	49.5	28.4
III-A/0.5 mm	76.9	0.35	1140	376	130.2	1.7	33	77.5	25.6
III-B/0.5 mm	102.6	0.37	855	365	124.5	1.2	42.5	58.1	24.8

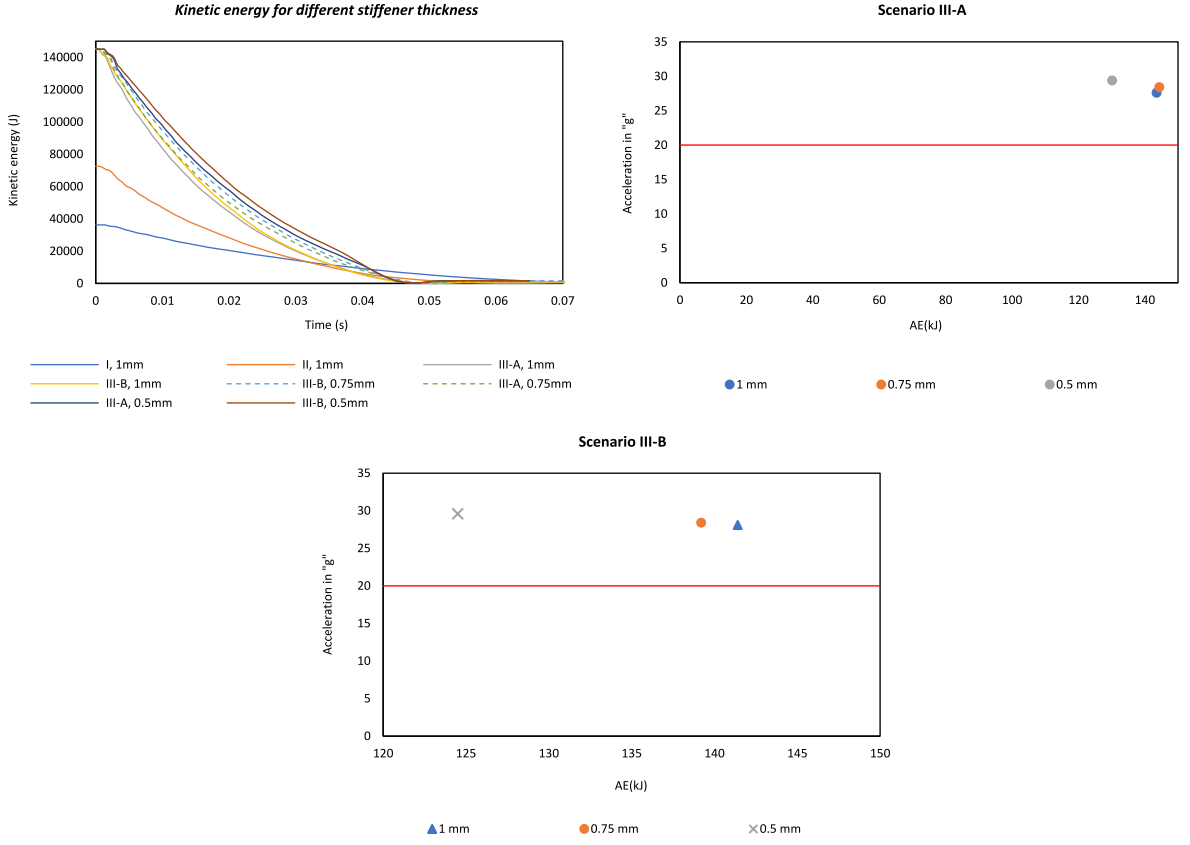


Fig. 26. KE evolution and comparison of AE and mean acceleration for various stiffener thicknesses and scenarios.

direction scenarios. In the L-direction, the foam-filled design with a 1 mm sheet thickness excelled.

Incorporating stiffeners improves structural integrity, expands absorbed energy, and tailors crash behaviour for L-direction crashes. A minimum stiffener thickness between 0.5 and 0.75 mm is suggested to avoid densification compromising crashworthiness by reducing the energy absorption effectiveness. Stiffeners significantly influence L-direction forces and absorbed energy, causing greater oscillations than in T-direction. Stiffeners and foam enhance absorbed energy but increase accelerations while varying wall thickness effectively reduces acceleration and SEA due to lightweight structural mass.

In the T-direction, optimisation may explore cell wall thicknesses (0.23–1 mm) with aluminium foam, identifying optimal positions for reduced PA and MA, while enhancing absorbed energy and SEA. The 0.23 mm empty cell design achieved MA<20g, contrasting with the 1 mm thick foam-filled cell design exceeding 20g. T-direction impacts do not consider internal air pressure in closed cells. Future research should assess remaining structure energy absorption without endangering occupants, establishing minimum acceptable absorbed energy, and favouring alternative honeycomb designs. Further research might explore similar honeycomb crash boxes with composite materials, comparing collapse behaviour under diverse conditions, demonstrating achievable crashworthiness criteria with innovative honeycomb designs integrating stiffeners, foam, or variable wall thicknesses.

Funding

Grant No. TP1288 is supported by the Royal Academy of Engineering (RAE) through the Engineering X Transforming Systems through Partnership programme.

Institutional Review Board Statement: N/A.

Informed Consent Statement: N/A.

CRediT authorship contribution statement

A. De Biasio: Writing – original draft, Validation, Software, Methodology, Formal analysis. **H. Ghasemnejad:** Writing – review & editing, Supervision, Resources, Investigation, Conceptualization. **S. Srimanosaowapak:** Writing – review & editing, Supervision. **J.W. Watson:** Conceptualization.

Declaration of competing interest

Submission of this article implies that the work described has not been published previously, that it is not under consideration for publication elsewhere, that its publication is approved by all authors and tacitly or explicitly by the responsible authorities where the work was carried out, and that, if accepted, it will not be published elsewhere in the same form, in English or in any other language, including electronically without the written consent of the copyright-holder.

Data availability

Data will be made available on request.

Acknowledgments

This research was carried out in collaboration with the industry partner, Bangkok Expressway and Metro Public Company Ltd., and the Thai research center, National Metal and Materials Technology Center (MTEC). This work was also sponsored by the Royal Academy of Engineering (RAE) through the Engineering X Transforming Systems through Partnership programme. All funding resources are acknowledged.

References

Aktay, L., Johnson, A.F., Kröplin, B.H., 2008. Numerical modelling of honeycomb core crush behaviour. Eng. Fract. Mech. 75 (9), 2616–2630. https://doi.org/10.1016/j.engfracmech.2007.03.008.

Betts, C., Lin, J., Balint, D., Atkins, A., 2012. 2D FE micromechanics modelling of honeycomb core sandwich panels. Eng. Trans. 60 (3).

Bitzer, T., 1997. Honeycomb Technology. Springer, Netherlands. https://doi.org/10.1007/978-94-011-5856-5.

Fleck, N., 2016. Metal Foams : a Design Guide Etal Foams : A Design Guide, vol. 3069.

Garai, F., Béres, G., Weltsch, Z., 2020. Development of tubes filled with aluminium foams for lightweight vehicle manufacturing. Materials Science and Engineering: A 790, 139743. https://doi.org/10.1016/j.msea.2020.139743.

Gibson, L.J., 2003. Cellular solids. MRS Bull. 28 (4), 270–274. https://doi.org/10.1557/MRS2003.79.

Güden, M., Kavi, H., 2006. Quasi-static axial compression behavior of constraint hexagonal and square-packed empty and aluminum foam-filled aluminum multi-tubes. Thin-Walled Struct. 44 (7), 739–750. https://doi.org/10.1016/j.tws.2006.07.003.

Hanssen, A.G., Langseth, M., Hopperstad, O.S., 2000. Static and dynamic crushing of square aluminum extrusions with aluminum foam filler. Int. J. Impact Eng. 24 (4) https://doi.org/10.1016/S0734-743X(99)00169-4.

He, Q., Ma, D.W., 2015. Parametric study and multi-objective crashworthiness optimisation of reinforced hexagonal honeycomb under dynamic loadings. Int. J. Crashworthiness 20 (5), 495–509. https://doi.org/10.1080/13588265.2015.1041324.

Langseth, M., Hopperstad, O.S., 1996. Static and dynamic axial crushing of square thin-walled aluminium extrusions. Int. J. Impact Eng. 18 (7–8) https://doi.org/10.1016/s0734-743x(96)00025-5.

Langseth, M., Berstad, T., Hopperstad, O.S., Clausen, A.H., 1994. Energy absorption in axially loaded square thin-walled aluminium extrusions. WIT Trans. Built Environ. 8.

Langseth, M., Hopperstad, O.S., Hanssen, A.G., 1998. Crash behaviour of thin-walled aluminium members. Thin-Walled Struct. 32 (1–3), 127–150. https://doi.org/10.1016/S0263-8231(98)00030-5.

Li, Z., Yu, J., Guo, L., 2012. Deformation and energy absorption of aluminum foam-filled tubes subjected to oblique loading. Int. J. Mech. Sci. 54 (1), 48–56. https://doi.org/10.1016/j.ijmecsci.2011.09.006.

Lu, G., Yu, T., 2003. Energy Absorption of Structures and Materials. https://doi.org/10.1533/9781855738584.

Nicoud, G., 2022. Development of Aluminium Crashbox for Crashworthiness Performance. Cranfield University, Cranfield.

Nicoud, G., Ghasemnejad, H., Srimanosaowapak, S., Watson, J.W., 2023. Crashworthiness of foam-filled and reinforced honeycomb crash absorbers in transverse direction. Appl. Compos. Mater. https://doi.org/10.1007/s10443-023-10181-1.

Pandarkar, A., Goel, M.D., Hora, M.S., 2016. Axial crushing of hollow and foam filled tubes: an overview. Sadhana - Acad. Proc. Eng. Sci. 41 (8), 909–921. https://doi.org/10.1007/s12046-016-0525-4.

Rai, V., Ghasemnejad, H., Watson, J.W., Gonzalez-Domingo, J.A., Webb, P.F., 2019. Developed trigger mechanisms to improve crush force efficiency of aluminium tubes. Eng. Struct. 199 https://doi.org/10.1016/j.engstruct.2019.109620.

Rajak, D.K., Kumaraswamidhas, L.A., Das, S., 2014. An energy absorption behaviour of foam filled structures. Procedia Materials Science 5, 164–172. https://doi.org/10.1016/j.mspro.2014.07.254.

Ramamurty, U., Paul, A., 2004. Variability in mechanical properties of a metal foam. Acta Mater. 52 (4), 869–876. https://doi.org/10.1016/J.ACTAMAT.2003.10.021.

Srinath, G., Vadiraj, A., Balachandran, G., Sahu, S.N., Gokhale, A.A., 2010. Transactions of the Indian Institute of Metals Characteristics of Aluminium Metal Foam for Automotive Applications, vol. 63, pp. 765–772 [Online]. Available: www.springerlink.com. (Accessed 14 March 2023).

Valente, G., 2021. Development of Aluminium Crashbox for Crashworthiness Performance. Cranfield University, Cranfield.

Valente, G., Ghasemnejad, H., Srimanosaowapak, S., Watson, J.W., 2023. Advancement in design and failure analysis of aluminium foam-filled honeycomb crash absorbers. Appl. Compos. Mater. https://doi.org/10.1007/s10443-023-10116-w.

Wang, Y., Zhang, R., Liu, S., Zhai, X., Zhi, X., 2021. Energy absorption behaviour of an aluminium foam-filled circular-triangular nested tube energy absorber under impact loading. Structures 34. https://doi.org/10.1016/j.istruc.2021.07.065.

Wierzbicki, T., 1983. Crushing Analysis of Aluminium Honeycomb 1, 157–174.

Wu, E., Jiang, W.S., 1997. Axial crush of metallic honeycombs. Int. J. Impact Eng. 19 (5–6), 439–456. https://doi.org/10.1016/s0734-743x(97)00004-3.

Yamashita, M., Gotoh, M., 2005. Impact behavior of honeycomb structures with various cell specifications - numerical simulation and experiment. Int. J. Impact Eng. 32 (1–4), 618–630. https://doi.org/10.1016/j.ijimpeng.2004.09.001.

Yuen, S.C.K., Nurick, G.N., 2008. The energy-absorbing characteristics of tubular structures with geometric and material modifications: an overview. Appl. Mech. Rev. 61 (1–6) https://doi.org/10.1115/1.2885138.

Zarei Mahmoudabadi, M., Sadighi, M., 2011. A study on the static and dynamic loading of the foam filled metal hexagonal honeycomb - theoretical and experimental. Mater. Sci. Eng. 530 (1), 333–343. https://doi.org/10.1016/j.msea.2011.09.093.

Zhang, C.J., Feng, Y., Bin Zhang, X., 2010. Mechanical properties and energy absorption properties of aluminum foam-filled square tubes. Trans. Nonferrous Metals Soc. China 20 (8), 1380–1386. https://doi.org/10.1016/S1003-6326(09)60308-3.



https://dspace.org/

Development of multi aluminium foam-filled crash box systems to improve crashworthiness performance of road Service vehicle

De Biasio, Antony; Ghasemnejad, Hessam; Srimanosaowapak, S.; Watson, James W.

2025-01
Elsevier
https://doi.org/10.1016/j.euromechsol.2024.105433
De Biasio A, Ghasemnejad H, Srimanosaowapak S, Watson JW. (2025) Development of multi aluminium foam-filled crash box systems to improve crashworthiness performance of road Service vehicle. European Journal of Mechanics - A/Solids, Volume 109, January-February 2025, Article number 105433

Downloaded from a DSpace repository. https://dspace.org/